Theoretical Explanation of Nonexponential OH Decay in Reactions with Benzene and Toluene under Pseudo-First-Order Conditions

Víctor Hugo Uc,[†] J. Raúl Alvarez-Idaboy,*[,‡] Annia Galano,[†] and Annik Vivier-Bunge[†]

Departamento de Química, Universidad Autónoma Metropolitana, Iztapalapa, México D.F., 09340 México, and Facultad de Química, Departamento de Física y Química Teórica, Universidad Nacional Autónoma de México, México D.F., 04510 México

Received: March 26, 2008; Revised Manuscript Received: June 8, 2008

OH radical reactions with benzene and toluene have been studied in the 200−600 K temperature range via the CBS-QB3 quantum chemistry method and conventional transition-state theory. Our study takes into account all possible hydrogen abstraction and OH-addition channels, including ipso addition. Reaction rates have been obtained under pseudo-first-order conditions, with aromatic concentrations in large excess compared to OH concentrations, which is the case in the reported experiments as well as in the atmosphere. The reported results are in excellent agreement with the experimental data and reproduce the discontinuity in the Arrhenius plots in the 300 K < T < 400 K temperature range. They support the suggestion that the observed nonexponential OH decay is caused by the existence of competing addition and abstraction channels and by the decomposition of thermalized OH−aromatic adducts back to reactants. We also find that the low-temperature onset of the nonexponential decay depends on the concentration of the aromatic compounds and that the lower the concentration, the lower the temperature onset. Under atmospheric conditions, nonexponential decay was found to occur in the 275−325 K range, which corresponds to temperatures of importance in tropospheric chemistry. Branching ratios for the different reaction channels are reported. We find that for $T \geq 400$ K the reaction occurs exclusively by H abstraction. At 298 K, ipso addition contributes 13.0% to the overall OH + toluene reaction, while the major products correspond to ortho addition, which represents 43% of all possible channels.

Introduction

Kinetics and mechanisms associated with the atmospheric oxidation of aromatic compounds are important in the chemistry of urban and regional atmospheres. These contaminants are emitted into the troposphere mainly from anthropogenic sources, and they account for 20−30% of non-methane hydrocarbons in urban air.[1] Their major atmospheric loss process during daylight hours is their reaction with hydroxyl radicals (OH),[2] which proceeds by H abstraction from the alkyl group and by OH addition to the aromatic ring.[3,4] It has been established that, at room temperature and atmospheric pressure, the formation of OH−aromatic adducts accounts for more than 90% of the overall reaction in the case of benzene and toluene.[5]

In their classical book on atmospheric chemistry, Finlayson-Pitts and Pitts[6] have summarized the mechanism and observed kinetics of aromatic molecules reacting with OH radicals. Three distinct regions can be observed in Arrhenius plots of log k versus 1000/T. At low temperatures, below ∼325 K, the plot is linear but with a slope that is negative for benzene and positive for toluene. At temperatures above ∼380 K, a linear plot is obtained with a negative slope, typical of a normal Arrhenius behavior. Between these two temperatures, a nonexponential decay is observed[7,8] and the Arrhenius plot presents an abrupt discontinuity. There are no recommended values for the rate constants in this region.

The existence of the positive slope in the low-temperature region in the toluene reaction, which implies that the observed activation energy is negative, can be explained in terms of a complex mechanism that has been discussed elsewhere.[9] The nonexponential OH decay in the intermediate temperature region, as well as the unusual Arrhenius plots, have been rationalized on the basis of two types of reaction paths, addition and abstraction, occurring simultaneously. It has been postulated that the thermalized OH−aromatic adduct formed by the OH radical addition to the ring decomposes back to reactants,[8] thus decreasing the importance of the addition channel and leading to bimolecular reaction rate-constant values significantly lower than those measured near room temperature. However, computational kinetics calculations using quantum chemistry data for these reactions under pseudo-first-order conditions have not been used to account for the observed Arrhenius plots. Suh et al.[10] have performed B3LYP/6-31G(d,p) calculations for the OH + toluene reaction and concluded that the equilibrium constant at 1 atm and 299 K indicates that unimolecular decomposition of the OH−toluene adduct is too slow to compete with bimolecular recombination. However, this temperature falls out of the interval where the adduct decomposition is assumed to occur.

In general, only addition to ortho, meta, and para positions has been considered in laboratory studies for OH/aromatic systems. Yet only about 70% of the reacted carbon has been fully accounted for.[11] Thus, pathways involving the initial formation of ipso adducts might also play a nonnegligible role in the laboratory and tropospheric chemistry of aromatic compounds. In fact, Trayham[12] has described numerous examples of ipso free radical substitution and he emphasized the

* To whom correspondence should be addressed: e-mail jidaboy@servidor.unam.mx.
[†] Universidad Autónoma Metropolitana.
[‡] Universidad Nacional Autónoma de México.

10.1021/jp8026258 CCC: $40.75
Published on Web 07/29/2008

importance of the ipso position in free radical reactions with aromatic hydrocarbons. Tiecco[13] has shown that radical additions to ipso sites can be equally important, or even more important, than the addition to the nonsubstituted C sites of aromatic compounds. In previous works from our group, isomeric adduct stability in the addition of H, O(^{3}P), F, and Cl to toluene[14] and xylenes[15] has been discussed, and we have shown that ipso addition is clearly favored for F radicals. Several recent calculations have emphasized the possible role of ipso adducts in toluene,[16] xylenes,[17,18] and phenol.[19] Rather than a steric hindrance, stabilization due to interactions between the lone pair on the oxygen atom and two methyl hydrogen atoms has been described in some of these studies. Details of the systems studied and the major results published in the literature have been summarized in a recent review.[20]

In this work, quantum chemistry and computational kinetics calculations will be used in the 200−600 K temperature range to study the OH reactions with benzene and toluene. All possible H abstraction and addition channels, including ipso addition, will be taken into account, and the same methods will be employed for all channels. We will use a theoretical approach that is in line with both experimental and environmental conditions and that takes into account the fact that aromatic concentrations are in large excess compared to OH concentrations. Thus, pseudo-first-order kinetics will be used to describe the addition reactions, and the possibility of the reverse reaction will be explicitly introduced. Branching ratios will be obtained for all channels.

Computational Methodology

Electronic structure calculations have been performed with the Gaussian 03 program.[21] The high-level composite method CBS-QB3[22] has been used for all the calculations. The complete basis set (CBS) models are compound methods that extrapolate to the CBS limit by using asymptotic convergence of MP2 pair energies calculated from pair natural orbital expansions.[22,23] They were developed to overcome the truncation of the basis sets, which is a major source of error in quantum mechanical calculations. CBS-QB3 is a five-step method that starts with B3LYP geometry and frequency calculations, followed by CCSD(T), MP4SDQ, and MP2 single-point calculations and a CBS extrapolation.[22] It also corrects for spin contamination, an important issue in OH addition reactions to unsaturated compounds.

In all cases, the character of the stationary points was confirmed by analyzing the frequency calculations: only positive eigenvalues for minima and one negative eigenvalue (imaginary frequency) for transition states. It was verified that the motion along the reaction coordinate corresponds to the expected transition vector.

Rate constants were obtained in the temperature range 200−600 K, by conventional transition-state theory (TST)[24–26] as implemented in TheRate program[27] at the Computational Science and Engineering Online Web site (www.cseo.net).[28]

For the calculation of the rate constants (k), a complex mechanism has been proposed for many radical−molecule reactions[9,29–33] and particularly for radical additions to unsaturated compounds.[34–36] It involves a fast pre-equilibrium between the isolated reactants and a reactants complex (RC), followed by an irreversible step leading to the formation of products. In a classical treatment, the calculation of the overall rate coefficient depends only on the properties of reactants and transition states, and it can be shown that the RC energy and partition function cancels out in the rate constant expression.[37] However, when there is a possibility of quantum mechanical tunneling, the existence of the reactant complex implies that the actual barrier is higher and that there are additional energy levels from where tunneling may occur; thus the tunneling factor increases. It should be noticed that this is used since the studied reactions are at the high-pressure limit. Accordingly, one can ignore reactant complexes in addition channels, but they are essential for the correct calculation of H abstraction rate constants.

SCHEME 1

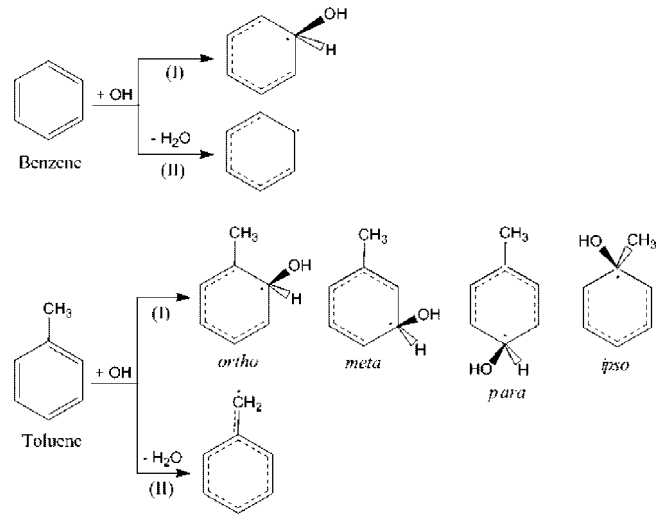

Scheme I

Results and Discussion

Two different kinds of reaction paths have been considered: (I) OH additions to the ring and (II) H abstractions. For benzene there are only two different paths since all the C sites are perfectly equivalent. For toluene, on the other hand, there are four possible nonequivalent additions depending on the position of the OH attack—ortho, meta, para, and ipso—while H abstraction is expected to occur almost exclusively from the methyl group[38] (Scheme 1).

Geometries. The optimized geometries of the transition states (TS) involved in all modeled reaction paths are shown in Figure 1, where the most relevant geometrical parameters have been indicated. According to the Hammond postulate,[39] the earlier the TS, the lower the heat of reaction. When the TS structures for the addition channels are compared, it can be noticed that the latest one (i.e., the most productlike) is the one for benzene, which has the shortest O···C distance. This suggests that the less exothermic channel should correspond to OH addition to benzene. This finding is in line with the common knowledge that methyl substituent groups activate the reactivity of the ring with respect to OH radical attacks. From the structures of the transition states involving toluene, it can be inferred that meta channels should be those least likely to occur among the addition reactions, while ortho adducts are expected to be the most abundant ones, at least at room temperature. Comparisons of the TS geometries involved in H abstraction reactions (path II) are not straightforward since the distances of the forming O···H and breaking C···H bonds are both significantly longer in the TS-II structure involving benzene. The L parameter has been calculated. This parameter not only denotes if a TS structure is reactantlike ($L < 1$) or productlike ($L > 1$) but also quantifies the corresponding trend. It has been calculated for each H abstraction, following refs 40 and 41, as

$$L = \frac{\delta r(\mathrm{C-H})}{\delta r(\mathrm{H-O})} \quad (1)$$

where δr(C−H) represents the variation in the breaking bond distance between transition states and reactants and δr(H−O) stands for the variation in the forming bond distance between transition states and products. The calculated values are L^{II}(benzene) = 0.61 and L^{II}(toluene) = 0.08. Accordingly, all the H abstractions are expected to be exothermic, although significantly less for benzene (aromatic abstractions) than for toluene (aliphatic abstractions).

Energies. CBS-QB3 Gibbs free energies of reaction (ΔG) and barriers ($\Delta G^{\ddagger}$) at room temperature are reported in Table 1. All the modeled reaction paths were found to be exergonic ($\Delta G < 0$), in agreement with the geometrical features of the transition states discussed above; that is, all of them are reactantlike (early) transition states. When the ΔG values for the H abstraction channels are compared, it can be noticed that the path involving abstractions from the ring (benzene) is significantly less exergonic than the one involving the methyl group in toluene. Regarding OH additions to toluene, the largest exergonicity was found for the formation of ortho and ipso adducts. Accordingly, the relationship between the earliness of the transition states and the ΔG values is very well observed.

Upon analysis of the Gibbs free energy barriers, it becomes evident that while for benzene the channel with the lowest barrier is also the most exergonic one, for toluene no direct correspondence between these two magnitudes is observed. In fact, for toluene, the H abstraction channel is the most exergonic one, but it is also the one with the highest barrier. Among the OH additions to toluene, the formation of the ipso adducts is the most exergonic channel, while its barrier is third in increasing order of height. Therefore, for substituted aromatic compounds, Gibbs free energies of reaction are definitely not an adequate criterion for predicting the relative importance of different channels. It is imperative to compute transition states and to calculate energy barriers in terms of Gibbs free energies, since the entropy evolution may vary for different paths. This explains why previous theoretical work based only on heats of reaction always found ipso adducts to be as important as ortho adducts, in contradiction with the available experimental evidence.

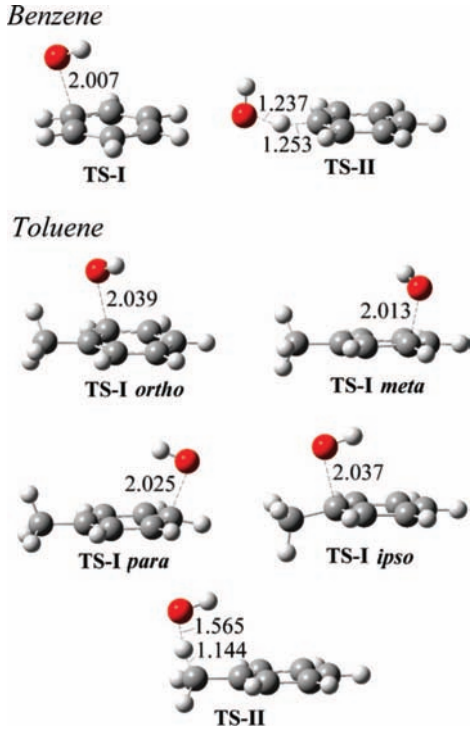

Figure 1. Optimized geometries of the transition states.

TABLE 1: CBS-QB3 (ΔG) and Barriers ($\Delta G^{\ddagger}$) at Room Temperature

	ΔG (kcal/mol)	$\Delta G^{\ddagger}$ (kcal/mol)
benzene		
I	−10.35	8.89
II	−5.84	11.80
toluene		
I ortho	−10.57	8.15
I meta	−9.46	8.69
I para	−8.97	8.25
I ipso	−10.68	8.43
II	−28.20	9.09

TABLE 2: Comparison between Calculated and Experimental Arrhenius Parameters within the 250−400 K Temperature Range of Pre-exponential Factor A and Activation Energy E_a

	adduct formation (bimolecular)		adduct decomposition	
	A (cm^3 molecule^{-1} s^{-1})	E_a (kcal/mol)	A (s^{-1})	E_a (kcal/mol)
benzene				
calc	5.2×10^{-12}	0.71	4.7×10^{13}	19.47
ref 7	4.0×10^{-11}	0.91 ± 1.0	3×10^{13}	18.70 ± 1.00
ref 8	3.1×10^{-12}	0.53 ± 0.43		
ref 52	6.3×10^{-12}	1.00 ± 0.10	4×10^{13}	18.88 ± 0.72
ref 53			3×10^{13}	17.80 ± 0.69
ref 50	2.3×10^{-12}	0.38 ± 0.12	3×10^{13}	16.25 × 0.72
ref 54	1.3×10^{-12}	0.00	3×10^{13}	19.00
ref 55	3.4×10^{-13}	0.70 ± 0.18	9×10^{12}	17.03 ± 0.34
toluene				
calc	1.48×10^{-12}	−0.56	6.1×10^{14}	20.90

Kinetics. The rate coefficients have been calculated within the temperature range 200−600 K. We have assumed that neither mixing nor crossover between different pathways occurs and that the overall rate constant (k) corresponding to each aromatic compound + OH can be calculated as the sum of the rate coefficients of each path:

$$k^{\mathrm{overall}}(\mathrm{benzene}) = k_{(\mathrm{I})} + k_{(\mathrm{II})} \quad (2)$$

$$k^{\mathrm{overall}}(\mathrm{toluene}) = k_{(\mathrm{I\ ortho})} + k_{(\mathrm{I\ meta})} + k_{(\mathrm{I\ para})} + k_{(\mathrm{I\ ipso})} + k_{(\mathrm{II})} \quad (3)$$

As mentioned before, in H abstraction channels, tunneling effects might be significant and the existence of the reactant complexes must be taken into account. Therefore, for paths II, a complex mechanism has been modeled involving a fast pre-equilibrium between the isolated reactants and a reactant complex (step 1), followed by an irreversible step (step 2) leading to products formation:

$$\text{Step 1:}\quad \mathrm{OH} + \mathrm{arom} \underset{k_{-1}}{\overset{k_1}{\rightleftharpoons}} [\mathrm{OH} \cdots \mathrm{arom}]$$

$$\text{Step 2:}\quad [\mathrm{OH} \cdots \mathrm{arom}] \xrightarrow{k_2} \mathrm{products}$$

According to this mechanism, if k_1 and k_{-1} are the forward and reverse rate constants for the first step and k_2 corresponds to the second step, a steady-state analysis leads to a rate coefficient for the overall reaction channel that can be written as

$$k = \frac{k_1 k_2}{k_{-1} + k_2} \quad (4)$$

Even though the energy barrier for k_{-1} is about the same height as that for k_2, the entropy change is much larger in the reverse reaction than in the formation of the products. Thus, k_{-1} is expected to be considerably larger than k_2. On the basis of this assumption, first considered by Singleton and Cvetanovic,[42] k can be rewritten as

$$k_{II} = \frac{k_1 k_2}{k_{-1}} = K_{eq} k_2 \quad (5)$$

where K_{eq} is the equilibrium constant between the isolated reactants and the reactant complex and k_2 is the rate constant corresponding to the second step of the mechanism, that is, to the transformation of the reactant complex into products. We have assumed that the reactant complex undergoes collisional stabilization, that is, the reaction occurs at the high-pressure limit. We have used this limit as our working hypothesis, since there is no experimental evidence that indicates otherwise. In fact it has been established that the high-pressure limit is reached at 100 Torr.[8] This approach has been previously used to describe OH radical reactions with several volatile organic compounds (VOCs).[37,43–46] It is also adequate to account for the experimental negative activation energy observed for OH reactions with toluene.[47–49]

For addition paths I, although reactant complexes also exist, they can be ignored in the rate constant calculation because no tunneling effect is expected. We have assumed that an equilibrium is established between the reactants and the adduct:

$$OH + arom \underset{k_{-3}}{\overset{k_3}{\rightleftharpoons}} [adduct]$$

k_3 and k_{-3} have been calculated as

$$k_3 = \sigma \frac{k_B T}{h} e^{-(\Delta G_3^{\ddagger})/RT} \quad (6)$$

$$k_{-3} = \sigma \frac{k_B T}{h} e^{-(\Delta G_{-3}^{\ddagger})/RT} \quad (7)$$

where k_B and h are the Boltzmann and Planck constants, $\Delta G^{\ddagger}$ is the Gibbs free energy of activation ($G_{TS} - G_R$), and σ represents the reaction path degeneracy, which accounts for the number of equivalent reaction paths.

The calculated Arrhenius parameters corresponding to adduct formation and decomposition, within the 250−400 K temperature range, are compared to the available experimental data in Table 2. Some experimental studies use a biexponential function to extract the information on forward and backward reactions,[50,51] while they are directly calculated in this work. For benzene + OH reaction, the experimental activation energies corresponding to adduct formation range from 0.38 to 1.00 kcal/mol and the calculated value was found to be equal to 0.71 kcal/mol. For the adduct decomposition, the experimental values range from 16.2 to 19.0 kcal/mol, and the value obtained from the present calculations was found to be slightly overestimated at about 19.5 kcal/mol. Accordingly, there is good agreement between the calculated values and those estimated from experimental data.

The observed rate for the addition reactions is

$$v = -\frac{d[arom]}{dt} = -\frac{d[OH]}{dt} = \frac{d[adduct]}{dt} = k_3[arom][OH] - k_{-3}[adduct] \quad (8)$$

However, under both experimental and environmental conditions, [arom] ≫ [OH], and the reaction occurs in pseudo-first-order regime, so eq 8 becomes

$$v = k_3'[OH] - k_{-3}[adduct] \quad (9)$$

where

$$k_3' = k_3[arom] \quad (10)$$

Initial concentrations of $[benzene]_0 = 1 \times 10^{13}$ molecule/cm^3 and $[toluene]_0 = 6 \times 10^{13}$ molecule/cm^3 have been used to mimic experimental conditions, and the corresponding equilibrium constants

$$K_e' = k_3'/k_{-3} \quad (11)$$

for the pseudo-first-order addition reactions are reported in Table 3 within the studied temperature range. As the values in this table show, for $T \leq 325$ K

TABLE 3: Equilibrium Constants (K_e') for Pseudo-First-Order Addition Paths[a] in the 200−600 K Temperature Range[b]

		toluene				
T	benzene	ipso	ortho	meta	para	global
200	3.51×10^{8}	3.38×10^{10}	3.22×10^{11}	5.36×10^{10}	5.36×10^{8}	2.00×10^{10}
250	2.78×10^{4}	6.77×10^{5}	5.19×10^{6}	1.79×10^{6}	2.28×10^{4}	3.06×10^{5}
275	9.05×10^{2}	1.34×10^{4}	9.47×10^{4}	4.26×10^{4}	5.84×10^{2}	5.58×10^{3}
298	6.48×10^{1}	6.50×10^{2}	4.33×10^{3}	2.39×10^{3}	3.45×10^{1}	2.58×10^{2}
300	5.25×10^{1}	5.11×10^{2}	3.39×10^{3}	1.90×10^{3}	2.75×10^{1}	2.03×10^{2}
325	$\mathbf{4.76 \times 10^{0}}$	3.26×10^{1}	2.04×10^{2}	1.38×10^{2}	$\mathbf{2.07 \times 10^{0}}$	1.25×10^{1}
350	$\mathbf{6.11 \times 10^{-1}}$	$\mathbf{3.10 \times 10^{0}}$	1.84×10^{1}	1.46×10^{1}	$\mathbf{2.26 \times 10^{-1}}$	$\mathbf{1.17 \times 10^{0}}$
375	$\mathbf{1.04 \times 10^{-1}}$	$\mathbf{4.06 \times 10^{-1}}$	$\mathbf{2.31 \times 10^{0}}$	$\mathbf{2.10 \times 10^{0}}$	3.31×10^{-2}	$\mathbf{1.53 \times 10^{-1}}$
400	2.21×10^{-2}	6.90×10^{-2}	$\mathbf{3.76 \times 10^{-1}}$	$\mathbf{3.86 \times 10^{-1}}$	6.18×10^{-3}	2.61×10^{-2}
425	5.69×10^{-3}	1.45×10^{-2}	7.62×10^{-2}	8.71×10^{-2}	1.41×10^{-3}	5.55×10^{-3}
450	1.71×10^{-3}	3.67×10^{-3}	1.85×10^{-2}	2.32×10^{-2}	3.78×10^{-4}	1.42×10^{-3}
475	5.87×10^{-4}	1.08×10^{-3}	5.25×10^{-3}	7.17×10^{-3}	1.17×10^{-4}	4.20×10^{-4}
500	2.25×10^{-4}	3.58×10^{-4}	1.69×10^{-3}	2.49×10^{-3}	4.08×10^{-5}	1.42×10^{-4}
525	9.49×10^{-5}	1.33×10^{-4}	6.09×10^{-4}	9.61×10^{-4}	1.57×10^{-5}	5.34×10^{-5}
550	4.35×10^{-5}	5.44×10^{-5}	2.42×10^{-4}	4.05×10^{-4}	6.63×10^{-6}	2.21×10^{-5}
575	2.14×10^{-5}	2.41×10^{-5}	1.04×10^{-4}	1.85×10^{-4}	3.02×10^{-6}	9.89×10^{-6}
600	1.12×10^{-5}	1.15×10^{-5}	4.83×10^{-5}	9.02×10^{-5}	1.47×10^{-6}	4.75×10^{-6}

[a] Calculated with $[benzene]_0 = 1 \times 10^{13}$ molecule/cm^3 and $[toluene]_0 = 6 \times 10^{13}$ molecule/cm^3. [b] The values highlighted in boldface type correspond to those cases where direct and reverse rate constants are of similar magnitude.

$$k_3' \gg k_{-3} \qquad (K_e' \gg 1)$$

while for $T \geq 400$ K

$$k_3' \ll k_{-3} \qquad (K_e' \ll 1)$$

These ranges correspond exactly to those at which OH exponential decays are observed. The apparent rate constant of addition reactions is expected to be $\sim k_3'$ at low temperatures and ~ 0 at high temperatures, while in the range 320 K $\leq T \leq$ 400 K both direct and reverse reactions are expected to occur to a significant extent. This supports the hypothesis that the nonexponential OH decays observed in the 300 K $< T <$ 400 K range are caused by partial decomposition of the thermalized OH−aromatic adducts back to reactants, as proposed by Tully et al.[8] It also means that in the temperature region where OH nonexponential decay occurs it is not possible to find a unique value for the rate constants.

The results in Table 3 indicate that, at the aromatic concentrations used in experimental conditions, for $T \leq 325$ K OH adducts are expected to be the main products of the benzene reaction, while for $T \geq 375$ K the main products should be those formed by H abstraction. Analogous results are obtained for the toluene + OH reaction, although several paths contribute to adduct formation. Additions are the main mechanisms at $T > 375$ K, and H abstraction is favored at $T < 400$ K. These results are in agreement with the experimental data.[8]

A different situation is observed under atmospheric conditions: the pseudo-first-order behavior is still present, but the aromatic concentrations ($[\text{benzene}]_0 = 1 \times 10^{10}$ molecule/cm^3 and $[\text{toluene}]_0 = 8 \times 10^{10}$ molecule/cm^3) are significantly lower than those used in experiments. The corresponding equilibrium constants are reported in Table 4. In this case, the OH nonexponential decay is predicted to occur at lower temperatures and in a narrower range: 275 K $\leq T \leq$ 300 K. This finding is relevant to atmospheric chemistry. It should be noticed that under actual atmospheric conditions these systems become much more complicated since adducts are likely to react also with other species, particularly with O_2, also in a reversible way.[56] However, the above discussion, even if not complete, would still be valid.

Let us analyze the values in Table 4 in detail. For benzene, at 275 K the equilibrium constant K_e' is almost equal to 1, which means that the largest possible adduct concentration is half the initial OH concentration. At temperatures ≤ 250 K, K_e' becomes significantly larger than 1 and most benzene adducts are expected to be the major reaction products. On the other hand, at temperatures ≥ 298 K, a large proportion of adducts decomposes back to reactants, and the major observed products of the OH + benzene reaction are those corresponding to H abstractions, provided that further reactions (usually with O_2) are not much faster than adduct decomposition. For the OH + toluene reaction, the analysis becomes more complicated since there are four different addition channels. In this case, OH addition yields the main products of the reaction at $T < 298$ K, and H abstraction products are favored at $T > 325$ K. If one compares these results with those obtained when the aromatic concentrations correspond to experimental conditions, it becomes clear that the turning point where H abstractions start to play an important role shifts toward lower temperatures when the reaction takes place in atmospheric conditions, that is, when the initial concentration of aromatic compounds is smaller.

At any reaction time, the hydroxyl concentration can be written as

$$[\text{OH}] = [\text{OH}]_0 - x[\text{OH}]_0 \tag{12}$$

where $[\text{OH}]_0$ is the initial concentration and x is a variable that measures the extent of reaction and lies in the $0 \leq x \leq 1$ range. In addition:

$$[\text{OH}]_0 = [\text{OH}] + [\text{adduct}] \tag{13}$$

Then eq 9 can be written as

$$v = \left(k_3' - k_{-3}\frac{x}{(1-x)}\right)[\text{OH}] \tag{14}$$

and the apparent rate coefficient for the addition paths is

$$k_{(I)}^{app} = k_3^{app} = k_3' - \frac{x}{(1-x)}k_{-3} \tag{15}$$

It is important to notice that this is not a true constant, since its value depends on the variable x, which changes as the reaction progresses. The values of x can be estimated from the initial OH decay rates, which have been measured for times up to 14

TABLE 4: Equilibrium Constants (K_e') for Pseudo-First-Order Addition Paths[a] in the 200−600 K Temperature Range[d]

		toluene				
T	benzene	ipso	ortho	meta	para	global
200	3.51×10^{5}	4.51×10^{7}	4.30×10^{8}	7.15×10^{7}	7.15×10^{5}	5.86×10^{7}
250	2.78×10^{1}	9.03×10^{2}	6.92×10^{3}	2.39×10^{3}	3.04×10^{1}	1.12×10^{3}
275	$\mathbf{9.05 \times 10^{-1}}$	1.78×10^{1}	1.26×10^{2}	5.68×10^{1}	$\mathbf{7.79 \times 10^{-1}}$	2.21×10^{1}
298	6.48×10^{-2}	$\mathbf{8.67 \times 10^{-1}}$	$\mathbf{5.78 \times 10^{0}}$	$\mathbf{3.19 \times 10^{0}}$	4.60×10^{-2}	$\mathbf{1.09 \times 10^{0}}$
300	5.25×10^{-2}	$\mathbf{6.82 \times 10^{-1}}$	$\mathbf{4.52 \times 10^{0}}$	$\mathbf{2.53 \times 10^{0}}$	3.67×10^{-2}	$\mathbf{8.57 \times 10^{-1}}$
325	4.76×10^{-3}	4.34×10^{-2}	$\mathbf{2.72 \times 10^{-1}}$	$\mathbf{1.84 \times 10^{-1}}$	2.76×10^{-3}	5.55×10^{-2}
350	6.11×10^{-4}	4.13×10^{-3}	2.46×10^{-2}	1.95×10^{-2}	3.01×10^{-4}	5.37×10^{-3}
375	1.04×10^{-4}	5.41×10^{-4}	3.07×10^{-3}	2.80×10^{-3}	4.41×10^{-5}	7.16×10^{-4}
400	2.21×10^{-5}	9.20×10^{-5}	5.01×10^{-4}	5.15×10^{-4}	8.24×10^{-6}	1.24×10^{-4}
425	5.69×10^{-6}	1.94×10^{-5}	1.02×10^{-4}	1.16×10^{-4}	1.88×10^{-6}	2.65×10^{-5}
450	1.71×10^{-6}	4.89×10^{-6}	2.47×10^{-5}	3.10×10^{-5}	5.04×10^{-7}	6.75×10^{-6}
475	5.87×10^{-7}	1.43×10^{-6}	7.00×10^{-6}	9.56×10^{-6}	1.56×10^{-7}	2.00×10^{-6}
500	2.25×10^{-7}	4.78×10^{-7}	2.26×10^{-6}	3.32×10^{-6}	5.44×10^{-8}	6.72×10^{-7}
525	9.49×10^{-8}	1.78×10^{-7}	8.13×10^{-7}	1.28×10^{-6}	2.10×10^{-8}	2.51×10^{-7}
550	4.35×10^{-8}	7.25×10^{-8}	3.22×10^{-7}	5.41×10^{-7}	8.84×10^{-9}	1.03×10^{-7}
575	2.14×10^{-8}	3.22×10^{-8}	1.39×10^{-7}	2.47×10^{-7}	4.02×10^{-9}	4.59×10^{-8}
600	1.12×10^{-8}	1.53×10^{-8}	6.43×10^{-8}	1.20×10^{-7}	1.96×10^{-9}	2.19×10^{-8}

[a] Calculated with $[\text{benzene}]_0 = 1 \times 10^{10}$ molecule/cm^3 and $[\text{toluene}]_0 = 8 \times 10^{10}$ molecule/cm^3. [d] The values highlighted in boldface type correspond to those cases where direct and reverse rate constants are of similar magnitude.

TABLE 5: Apparent Rate Coefficients[a]

	k^{app} (cm^3 molecule^{-1} s^{-1})	
T (K)	benzene	toluene
200	9.32×10^{-13}	7.39×10^{-12}
250	1.22×10^{-12}	4.83×10^{-12}
275	1.38×10^{-12}	4.37×10^{-12}
298	1.54×10^{-12}	4.14×10^{-12}
300	1.55×10^{-12}	4.13×10^{-12}
325	1.66×10^{-12}	3.71×10^{-12}
350	1.04×10^{-12}	3.01×10^{-12}
375	1.31×10^{-13}	1.33×10^{-12}
400	1.87×10^{-13}	8.89×10^{-13}
425	2.61×10^{-13}	1.04×10^{-12}
450	3.56×10^{-13}	1.19×10^{-12}
475	4.74×10^{-13}	1.36×10^{-12}
500	6.19×10^{-13}	1.55×10^{-12}
525	7.94×10^{-13}	1.74×10^{-12}
550	1.00×10^{-12}	1.94×10^{-12}
575	1.25×10^{-12}	2.16×10^{-12}
600	1.54×10^{-12}	2.39×10^{-12}

[a] Calculated with $[\text{benzene}]_0 = 1 \times 10^{13}$molecule/cm^3, $[\text{toluene}]_0 = 6 \times 10^{13}$ molecule/cm^3, and $t = 14$ ms.

ms.[7,8] The following expression can be obtained from the differential and integrated forms of k_3':

$$x = 1 - \frac{1}{\exp(k_3' t)} \tag{16}$$

and has been used in the present work to estimate the x values needed to calculate k_3^{app} in the studied temperature range.

Accordingly, the apparent bimolecular rate constants can be calculated from the pseudo-first-order rate constants as

$$k^{app}_{bimol}(\text{benzene}) = \frac{k^{app}_{(I)}}{[\text{benz}]_0} + k_{(II)} \tag{17}$$

$$k^{app}_{bimol}(\text{toluene}) = \frac{k^{app}_{(I\ ortho)}}{[\text{tol}]_0} + \frac{k^{app}_{(I\ meta)}}{[\text{tol}]_0} + \frac{k^{app}_{(I\ para)}}{[\text{tol}]_0} + \frac{k^{app}_{(I\ ipso)}}{[\text{tol}]_0} + k_{(II)} \tag{18}$$

The calculated values of the apparent bimolecular rate coefficients, calculated according to eqs 17 and 18 and corresponding to experimental conditions, are reported in Table 5. The recommended values[47] at 300 K are 1.30×10^{-12} and 6.12×10^{-12} cm^3 molecule^{-1} s^{-1} for benzene and toluene, respectively. The values calculated in this work, at the same temperature, differ from these by a factor of 1.2 for benzene and 1.5 for toluene. The excellent agreement with experiment validates the methodology used in the present work.

The branching ratios for the different studied channels of reaction are reported in Table 6 for the temperature range in which addition and abstraction contribute significantly to the overall reaction. They have been calculated as

$$\Gamma_{path} = \frac{k_{path}}{k_{overall}} \tag{19}$$

The values in Table 6 correspond to the following initial experimental conditions: $[\text{benzene}]_0 = 1 \times 10^{13}$ and $[\text{toluene}]_0 = 6 \times 10^{13}$ molecule/cm^3 and to measurements at time $t =$ 14 ms.

For the toluene reaction, at 298 K, ipso addition was found to contribute 13.0% to the overall reaction (Table 6). This contribution decreases as temperature increases, varying from 18% at 200 K to 0% at $T \geq 375$ K. Although small, it is

TABLE 6: Branching Ratios for All Modeled Paths of Reaction[a]

	benzene		toluene				
T (K)	Γ_I	Γ_{II}	$\Gamma_{I\ ortho}$	$\Gamma_{I\ meta}$	$\Gamma_{I\ para}$	$\Gamma_{I\ ipso}$	Γ_{II}
200	1.00	0.00	0.63	0.08	0.10	0.18	0.02
250	0.99	0.01	0.52	0.13	0.15	0.15	0.05
275	0.98	0.02	0.47	0.15	0.17	0.14	0.07
298	0.98	0.02	0.43	0.17	0.17	0.13	0.10
300	0.98	0.02	0.42	0.17	0.17	0.13	0.10
325	0.97	0.03	0.41	0.20	0.12	0.13	0.14
350	0.92	0.08	0.41	0.25	0.00	0.13	0.21
375	0.00	1.00	0.11	0.32	0.00	0.00	0.57
400	0.00	1.00	0.00	0.00	0.00	0.00	1.00

[a] Calculated with $[\text{benzene}]_0 = 1 \times 10^{13}$ molecule/cm^3, $[\text{toluene}]_0 = 6 \times 10^{13}$ molecule/cm^3, and $t = 14$ ms.

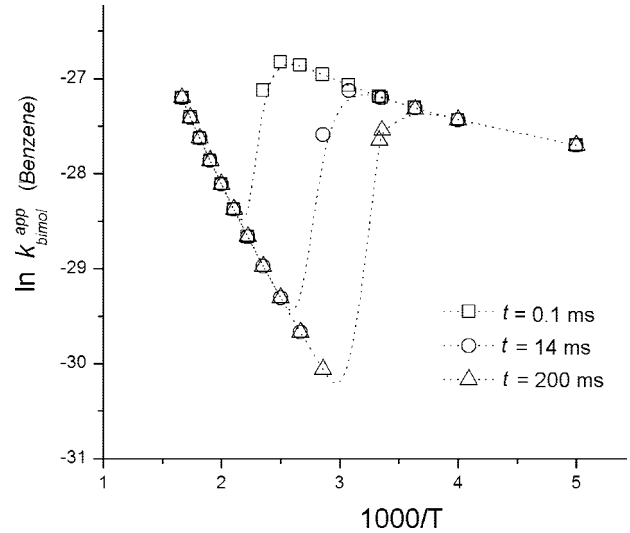

Figure 2. Temperature dependence of k^{app}(benzene) at $t = 0.1$, 14, and 200 ms, for pseudo-first-order conditions with $[\text{benzene}]_0 = 1 \times 10^{13}$ molecule/cm^3.

significant, and this suggests that the initial formation of ipso adducts plays a role in the tropospheric chemistry of aromatic compounds. The lack of experimental evidence on the ipso adducts can be explained by considering that, at room temperature, they are the least abundant addition products: 42% ortho, 17% meta, 17% para, and 13% ipso. In addition, it has been suggested that they isomerize to the ortho adduct. However, if ipso adducts were considered, the carbon unbalance between aromatic reactants and products could be significantly reduced.

Figure 2 shows the temperature dependence of k^{app}(benzene) at $t = 0.1$, 14, and 200 ms, for $[\text{arom}]_0 = 1 \times 10^{13}$ molecule/cm^3. The largest value of t is hypothetical and it has been included here for the sake of discussion. As this figure shows, the methodology used in this work reproduces the experimental behavior from refs 7 and 8. The abrupt drop in the temperature range where OH nonexponential decay is observed is reproduced here for the first time. This figure also shows that the temperature range at which the nonexponential decay occurs depends on the elapsed time from the beginning of the reaction, that is, on the advance of the reaction. This seems to be a logical result since the adduct concentration varies as the reaction progresses, thus altering the role of the reverse reaction (from adduct back to reactants). This finding also agrees with the predictions of Perry et al.[7] that if OH observations were performed on a shorter time scale, then the low-temperature onset of the nonexponential behavior would move up to higher temperatures. Actually, from our calculations, the low-temperature onset (T_{LO}) is predicted

to be around 325 K if $t = 14$ ms, which corresponds to the reported experimental values,[7,8] while it is ~400 K for $t = 0.1$ ms and ~275 K for $t = 200$ ms. The agreement with the results and predictions by Perry et al.[7] is remarkably good: these authors proposed $T_{LO} \sim 325$ K for $t \sim 1-30$ ms and $T_{LO} \sim 400$ K for $t \sim 10-100$ μs.

It should be noticed that similar time does not represent the same advance of reaction for different $[arom]_0$. Accordingly, there are two different ways of analyzing the low-temperature onset as $[arom]_0$ varies: at a fixed time or at a fixed advance of reaction. However, in the atmosphere, neither of these two magnitudes can be restrained. Actually, in the atmosphere the reaction progresses to time scales longer than 14 ms, which means that T_{LO} would be accordingly lowered and the H abstraction paths might start to contribute to the overall reaction at temperatures lower than those predicted from the experiments carried out up to date. This is in line with the predictions made on the basis of the pseudo-first-order equilibrium constant discussed above. It seems relevant to insist on the fact that this study is based on a simplified model from the actual atmospheric conditions, where other molecules are present and able to interact with the species involved in the studied reactions. It should also be noticed that using the same time for systems with different $[arom]_0$ is not expected to change the value of T_{LO} under pseudo-first-order conditions, since at a specific time t the system with higher $[arom]_0$ would also have the larger x and the two effects would cancel each other. For instance, $t =$ 14 ms would be equivalent to $x = 0.14$ for $[benzene]_0 = 1 \times 10^{13}$ molecule cm^{-3}, while $x = 0.0018$ for $[benzene]_0 = 1.2 \times 10^{10}$ molecule cm^{-3}. Accordingly, experimental product analysis using the actual atmospheric concentrations would be desirable in order to validate the predictions from this work.

Conclusions

Branching ratios based on Gibbs free energy barriers have been obtained for all channels in the 200−600 K range, and the role of the ipso addition channel has been clarified. The lack of experimental evidence for the ipso adducts can be explained by considering that they are expected to be the less abundant addition products. In addition, they may evolve into different species. However, at room temperature, their contribution is approximately 13%. Thus, if ipso adducts were taken into account, the carbon unbalance between aromatic reactants and products could be considerably reduced.

This study has been performed under pseudo-first-order conditions, with aromatic concentrations in large excess compared to OH concentrations as is the case both in previous experiments and in the atmosphere. Our results are in excellent agreement with the experimental data in the whole 200−600 K temperature range. They reproduce the observed nonexponential OH decay. The suggestion that the nonexponential OH decays observed in the 300 K $< T <$ 400 K range are caused by the decomposition of thermalized OH−aromatic adducts back to reactants and the competition between abstraction and addition channels is confirmed. The low-temperature onset of the nonexponential decay depends on the concentration of the aromatic compounds: the lower the concentration, the lower the temperature onset. This finding could have atmospheric implications since under atmospheric conditions the nonexponential decay was found to occur in the 275−325 K range, which corresponds to temperatures of importance in tropospheric chemistry.

Acknowledgment. We are thankful to the Mexican agency CONACYT through Grant SEP-2004-C01-46167 and to PIFI 3.3 for the acquisition of computer clusters. We thank the Dirección General de Servicios de Cómputo Académico (DGSCA) at Universidad Nacional Autónoma de México. This work was partially supported by a grant from the DGAPA UNAM (PAPIIT-IN203206). We also thank Professor P. H. Wine for providing detailed experimental data and Professor R. Atkinson for his valuable comments.

References and Notes

(1) Calvert, J. G.; Atkinson, R.; Becker, K. H.; Kamens, R. M.; Seinfeld, J. H.; Wallington, T. H.; Yarwood, G. *The mechanisms of atmospheric oxidation of aromatic hydrocarbons*; Oxford University Press: Oxford, U.K., 2002.

(2) Atkinson, R. *J. Phys. Chem. Ref. Data* **1994**, *Monograph 2*, 1.

(3) Molina, M. J.; Zhang, R.; Broekhuizen, K.; Lei, W.; Navarro, R.; Molina, L. T. *J. Am. Chem. Soc.* **1999**, *121*, 10225.

(4) Smith, D. F.; Kleindienst, T. E.; Mciver, C. D. *J. Atmos. Chem.* **1999**, *34*, 339.

(5) Atkinson, R. *J. Phys. Chem. Ref. Data* **1989**, *Monograph 1*, 1.

(6) Finlayson-Pitts, B. J.; Pitts, N. *Atmospheric Chemistry: Fundamentals and Experimental Techniques*; Wiley-Interscience: New York, 1986.

(7) Perry, R. A.; Atkinson, R.; Pitts, J. N. *J. Phys. Chem.* **1977**, *81*, 296.

(8) Tully, F. P.; Ravishankara, A. R.; Thompson, R. L.; Nicovlch, J. M.; Shah, R. C.; Kreutter, N. M.; Wine, P. H. *J. Phys. Chem.* **1981**, *85*, 2262.

(9) Singleton, D. L.; Cvetanovic, R. J. *J. Am. Chem. Soc.* **1976**, *98*, 6812.

(10) Suh, I.; Zhang, D.; Zhang, R.; Molina, L. T.; Molina, M. J. *Chem. Phys. Lett.* **2002**, *364*, 454.

(11) Atkinson, R.; Arey, J. *Chem. Rev.* **2003**, *103*, 4605.

(12) Trayham, J. G. *Chem. Rev.* **1979**, *79*, 323.

(13) Tiecco, M. *Acc. Chem. Res.* **1980**, *13*, 51.

(14) Uc-Rosas, V. H.; Grand, A.; Hernández-Laguna, A.; Vivier-Bunge, A. *Phys. Chem. Chem. Phys.* **2002**, *4*, 5730.

(15) Uc-Rosas, V. H.; Grand, A.; Hernández-Laguna, A.; Vivier-Bunge, A. *J. Mol. Struct. (THEOCHEM)* **2004**, *684*, 171.

(16) Uc, V. H.; García-Cruz, I.; Hernández-Laguna, A.; Vivier-Bunge, A. *J. Phys. Chem.* **2000**, *104*, 7847.

(17) Uc, V. H.; García-Cruz, I.; Vivier-Bunge, A. A theoretical study of the OH radical addition to the xylenes. In *Quantum Systems in Chemistry and Physics, Vol. II*; Hernández-Laguna, A., et al., Eds.; Advanced Problems and Complex Systems; Kluwer Academic Publishers: Dordrecht, The Netherlands, 2000; p 241−259.

(18) Fan, J. W.; Zhang, R. Y. M. *J. Phys. Chem. A* **2006**, *110*, 7728.

(19) Lundqvist, M. J.; Eriksson, L. A. *J. Phys. Chem. B* **2000**, *104*, 848.

(20) Andino, J.; Vivier-Bunge, A. Tropospheric Chemistry of Aromatic Compounds Emitted from Anthropogenic Sources. In *Advances in Quantum Chemistry, Vol. 55*; Goodsite, M. E., Johnson, M. S., Eds.; Applications of Quantum Chemistry to the Atmosphere; Elsevier: Amsterdam, 2008; Chapt. 14, pp 298−309.

(21) Frisch, M. J.; Trucks, G. W.; Schlegel, H. B.; Scuseria, G. E.; Robb, M. A.; Cheeseman, J. R.; Montgomery, J. A., Jr.; Vreven, T.; Kudin, K. N.; Burant, J. C.; Millam, J. M.; Iyengar, S. S.; Tomasi, J.; Barone, V.; Mennucci, B.; Cossi, M.; Scalmani, G.; Rega, N.; Petersson, G. A.; Nakatsuji, H.; Hada, M.; Ehara, M.; Toyota, K.; Fukuda, R.; Hasegawa, J.; Ishida, M.; Nakajima, T.; Honda, Y.; Kitao, O.; Nakai, H.; Klene, M.; Li, X.; Knox, J. E.; Hratchian, H. P.; Cross, J. B.; Bakken, V.; Adamo, C.; Jaramillo, J.; Gomperts, R.; Stratmann, R. E.; Yazyev, O.; Austin, A. J.; Cammi, R.; Pomelli, C.; Ochterski, J. W.; Ayala, P. Y.; Morokuma, K.; Voth, G. A.; Salvador, P.; Dannenberg, J. J.; Zakrzewski, V. G.; Dapprich, S.; Daniels, A. D.; Strain, M. C.; Farkas, O.; Malick, D. K.; Rabuck, A. D.; Raghavachari, K.; Foresman, J. B.; Ortiz, J. V.; Cui, Q.; Baboul, A. G.; Clifford, S.; Cioslowski, J.; Stefanov, B. B.; Liu, G.; Liashenko, A.; Piskorz, P.; Komaromi, I.; Martin, R. L.; Fox, D. J.; Keith, T.; Al-Laham, M. A.; Peng, C. Y.; Nanayakkara, A.; Challacombe, M.; Gill, P. M. W.; Johnson, B.; Chen, W.; Wong, M. W.; Gonzalez, C.; Pople, J. A. *Gaussian 03, revision D.01*; Gaussian, Inc.: Wallingford, CT, 2004.

(22) Montgomery, J. A.; Frisch, M. J.; Ochterski, J. W.; Petersson, G. A. *J. Chem. Phys.* **1999**, *110*, 2822.

(23) (a) Nyden, M. R.; Petersson, G. A. *J. Chem. Phys.* **1981**, *75*, 1843. (b) Al-Laham, M. A.; Petersson, G. A. *J. Chem. Phys.* **1991**, *94*, 6081. (c) Petersson, G. A.; Tensfeldt, T. G.; Montgomery, J. A. *J. Chem. Phys.* **1991**, *94*, 6091. (d) Petersson, G. A.; Malick, D. K.; Wilson, W. G.; Ochterski, J. W.; Montgomery, J. A.; Frisch, M. J. *J. Chem. Phys.* **1998**, *109*, 10570. (e) Montgomery, J. A.; Frisch, M. J.; Ochterski, J. W.; Petersson, G. A. *J. Chem. Phys.* **2000**, *112*, 6532.

(24) Eyring, H. *J. Chem. Phys.* **1935**, *3*, 107.

(25) Evans, M. G.; Polanyi, M. *Trans. Faraday Soc.* **1935**, *31*, 875.

(26) Truhlar, D. G.; Hase, W. L.; Hynes, J. T. *J. Phys. Chem.* **1983**, *87*, 2264.

(27) Duncan, W. T.; Bell, R. L.; Truong, T. N. *J. Comput. Chem.* **1998**, *19*, 1039.
(28) Zhang, S.; Truong, T. N. *VKLab, version 1.0*; University of Utah: Salt Lake City, UT, 2001.
(29) Mora-Diez, N.; Alvarez-Idaboy, J. R.; Boyd, R, J. *J. Phys. Chem. A* **2001**, *105*, 9034.
(30) Alvarez-Idaboy, J. R.; Mora-Diez, N.; Boyd, R, J.; Vivier-Bunge, A. *J. Am. Chem. Soc.* **2001**, *123*, 2018.
(31) Galano, A.; Alvarez-Idaboy, J. R.; Ruiz-Santoyo, M. E.; Vivier-Bunge, A. *ChemPhysChem* **2004**, *5*, 1379.
(32) Galano, A.; Alvarez-Idaboy, J. R.; Ruiz-Santoyo, M. E.; Vivier-Bunge, A. *J. Phys. Chem. A* **2005**, *109*, 169.
(33) Galano, A.; Alvarez-Idaboy, J. R. Atmospheric Reactions of Oxygenated Compounds + OH Radicals: Role of Hydrogen-Bonded Intermediates and Transition States. In *Advances in Quantum Chemistry, Vol. 55*; Goodsite, M. E., Johnson, M. S., Eds.; Applications of Quantum Chemistry to the Atmosphere; Elsevier: Amsterdam, 2008; Chapt. 12, pp 245−274.
(34) Alvarez-Idaboy, J. R.; Mora-Diez, N.; Vivier-Bunge, A. *J. Am. Chem. Soc.* **2000**, *122*, 3715.
(35) Francisco-Marquez, M.; Alvarez-Idaboy, J. R.; Galano, A.; Vivier-Bunge, A. *Phys. Chem. Chem. Phys.* **2003**, *5*, 1392.
(36) Francisco-Marquez, M.; Alvarez-Idaboy, J. R.; Galano, A.; Vivier-Bunge, A. *Chem. Phys.* **2008**, *344*, 273.
(37) Alvarez-Idaboy, J. R.; Cruz-Torres, A.; Galano, A.; Ruiz-Santoyo, M. E. *J. Phys. Chem. A* **2004**, *108*, 2740.
(38) Uc, V. H.; Alvarez-Idaboy, J. R.; Galano, A.; García-Cruz, I.; Vivier-Bunge, A. *J. Phys. Chem. A* **2006**, *110*, 10155.
(39) Hammond, G. S. *J. Am. Chem. Soc.* **1955**, *77*, 334.
(40) Rayez, M. T.; Rayez, J. C.; Sawerysyn, J. P. *J. Phys. Chem.* **1994**, *98*, 11342.
(41) Talhaoui, A.; Louis, F.; Devolder, P.; Meriaux, B.; Sawerysyn, J. P.; Rayez, M. T.; Rayez, J. C. *J. Phys. Chem.* **1996**, *100*, 13531.
(42) Singleton, D. L.; Cvetanovic, R. J. *J. Am. Chem. Soc.* **1976**, *98*, 6812.
(43) Alvarez-Idaboy, J. R.; Mora-Diez, N.; Vivier-Bunge, A. *J. Am. Chem. Soc.* **2000**, *122*, 3715.
(44) Alvarez-Idaboy, J. R.; Mora-Diez, N.; Boyd, R. J.; Vivier-Bunge, A. *J. Am. Chem. Soc.* **2001**, *123*, 2018.
(45) Galano, A.; Alvarez-Idaboy, J. R.; Bravo-Perez, G.; Ruiz-Santoyo, M. E. *Phys. Chem. Chem. Phys.* **2002**, *4*, 4648.
(46) Galano, A.; Alvarez-Idaboy, J. R.; Ruiz-Santoyo, M. E.; Vivier-Bunge, A. *J. Phys. Chem. A* **2002**, *106*, 9520.
(47) Atkinson, R. *Chem. Rev.* **1986**, *86*, 69.
(48) Bourmada, M.; Carlier, M.; Pauwels, J. F.; Devolder, P. *J. Chim. Phys.* **1988**, *85*, 881.
(49) Semadeni, M.; Stocker, D. W.; Kerr, J. A. *Int. J. Chem. Kinet.* **1995**, *27*, 287.
(50) Witte, F.; Urbanik, E.; Zetzsch, C. *J. Phys. Chem.* **1986**, *90*, 3251.
(51) See, for example, (a) ref 50. (b) Hynes, A. J.; Stoker, R. B.; Pounds, A. J.; McKay, T.; Bradshaw, J. D.; Nicovich, J. M.; Wine, P. H. *J. Phys. Chem.* **1995**, *99*, 16967. (c) Kulcke, A.; Blackmon, B.; Chapman, W. B.; Kim, I. K.; Nesbitt, D. J. *J. Phys. Chem. A.* **1998**, *102*, 1965. (d) Orlando, J. J.; Piety, C. A.; Nicovich, J. M.; McKee, M. L.; Wine, P. H. *J. Phys. Chem. A* **2005**, *109*, 6659.
(52) Lorenz, K.; Zellner, R. *Ber. Bunsen-Ges. Phys. Chem.* **1983**, *87*, 629.
(53) Wahner, A.; Zetzsch, C. *J. Phys. Chem.* **1983**, *87*, 4945.
(54) Wallington, T. J.; Neuman, D. M.; Kurylo, M. J. *Int. J. Chem. Kinet.* **1987**, *19*, 725.
(55) Knispel, R.; Koch, R.; Siese, M.; Zetzsch, C. *Ber. Bunsen-Ges. Phys. Chem.* **1990**, *94*, 1375.
(56) Koch, R.; Knispel, R.; Elend, M.; Siese, M.; Zetzsch, C. *Atmos. Chem. Phys.* **2007**, *7*, 2057.

JP8026258